Available online at www.sciencedirect.com
ScienceDirect
Journal of Magnetic Resonance 189 (2007) 104–113
JMR Journal of Magnetic Resonance
www.elsevier.com/locate/jmr

Stripline probes for nuclear magnetic resonance

P.J.M. van Bentum [a,*], J.W.G. Janssen [a], A.P.M. Kentgens [a,*], J. Bart [b], J.G.E. Gardeniers [b]

[a] Institute for Molecules and Materials, Radboud University, Toernooiveld 1, 6525ED Nijmegen, The Netherlands
[b] MESA+ Institute for Nanotechnology, University of Twente, Enschede, The Netherlands

Received 20 July 2007; revised 24 August 2007
Available online 7 September 2007

Abstract

A novel route towards chip integrated NMR analysis is evaluated. The basic element in the design is a stripline RF 'coil' which can be defined in a single layer lithographic process and which is fully scalable to smaller dimensions. The sensitivity of such a planar structure can be superior to that of a conventional 3D helix. The basic properties, such as RF field strength, homogeneity and susceptibility broadening are discussed in detail. Secondary effects related to the thermal characteristics are discussed in simplified models. Preliminary NMR tests of basic solid and liquid samples measured at 600 MHz confirm the central findings of the design study. It is concluded that the stripline structure can be a valuable addition to the NMR toolbox; it combines high sensitivity with low susceptibility broadening and high power handling capabilities in a simple scalable design.

Keywords: NMR; Microcoils; Stripline; Microfluidics; High resolution NMR; Thin films; Wide-line NMR; RF coil design

1. Introduction

Nuclear magnetic resonance (NMR) has become the analytical method of choice in many areas of research. The main bottleneck that impedes certain advancements in the field of NMR spectroscopy is the relatively low sensitivity of the NMR detection method. The Boltzmann factors that determine the thermodynamic population difference between nuclear spin levels lead to very low signal intensities. For routine NMR analysis one typically requires several cubic millimeters of sample with at least 10^{16} nuclear spins present. There are many potential applications where the NMR technique could provide invaluable information on local structure and dynamics but where sample volumes are prohibitively small. For example in the case of small (bio) crystals, oriented fibrils, membranes or thin epitaxial layers, traditional NMR probes are not well matched to the sample dimensions and the less than optimal filling factor of the RF detection coil leads to reduced signal to noise performance. It was suggested more than a decade ago that microcoil probes can achieve a much better filling factor and thus the limit of detection can be reduced to less than 10^{15} nuclear spins [1,2]. This represents about a factor 10 improvement in signal to noise for small mass-limited samples when compared to the common macroscopic NMR probes. Capillary microcoil probes with sample volumes of around 1 μl are now available commercially and have become competitive for a number of analytical applications [3]. Nevertheless, it is desirable to be able to work with even smaller sample volumes, as e.g. encountered in microfluidic devices. The present detection limit for NMR is at the nanomole level, while for example mass spectroscopy detection limits are many orders of magnitude lower and fluorescence techniques approach the single molecule level. Commercial microcoil probes are based on capillary sample chambers with a tightly wound helical RF coil wrapped around this capillary. The coil itself is immersed in a cylindrical chamber filled with susceptibility matching fluid to avoid the static field distortions by the copper helix [4,5]. Without the

* Corresponding authors. Fax: +31 24 3652112.
E-mail addresses: j.vanbentum@nmr.ru.nl (P.J.M. van Bentum), a.kentgens@nmr.ru.nl (A.P.M. Kentgens).

1090-7807/$ - see front matter © 2007 Elsevier Inc. All rights reserved.
doi:10.1016/j.jmr.2007.08.019

susceptibility matching, the spectroscopic resolution is seriously compromised. With the method of handmade discrete element assembly it is not easy to scale this design down in size.

Several groups have explored lithographic methods for microcoil production [6–10]. In a typical example, the RF coil is a planar helix and the sample chamber is incorporated in a microfluidic chip to achieve a versatile 'lab on a chip' with in-situ NMR analysis of reaction products and process dynamics. Despite many efforts, these approaches have not yet penetrated mainstream NMR spectroscopy. To a large extend this is due to some practical and some more fundamental limitations of these planar microcoil designs. In general, the B_1 field homogeneity for these planar helices is less than ideal and multidimensional NMR methods are more difficult to implement. Also, it is not easy to achieve a low loss connection to the inner electrode of the helix. RF shielding currents increase the effective resistance and this leads to higher noise factors. The most important problem is the fact that the nearby windings of the microcoil tend to induce static field distortions that limit both the resolution and the signal to noise performance. In order to realize the potential sensitivity gain in microcoil NMR these problems must be solved, preferably in an affordable way that allows for automated mass production. Recently we introduced a novel type of NMR 'coil', the stripline, that departs from the idea of a helical structure to generate RF B_1 fields and detect NMR signals [11]. The microslot design by Maguire and coworkers [12] is another appealing alternative to helical NMR coils. The basic philosophy behind the microslot approach is comparable to the present stripline approach. In both cases the rf current is carried by a thin strip of metal in close contact with the sample. The main difference is that in the stripline geometry there is a symmetric ground plane that confines the rf radiation. The boundary conditions impose a homogeneous current distribution and thus a homogeneous B_1 field. In the microslot case, discrete elements are used to create to form the resonator. The stripline concept presented here is based on quarter or half wavelength resonators that can in principle be constructed on chip with no discrete soldered elements in the resonating circuit. The prototype stripline probe presented here is a double tuned H/X. In the present contribution we concentrate on the basic principles of the stripline design, aiming to overcome the problems encountered with planar helix coils. Proof of principle will be given in the form of preliminary results with a prototype double resonant stripline probe. It is well known that stripline technology provides a versatile method to route high frequency signals with low losses and well-defined delay times on printed circuit boards and semiconductor chips. Basically, planar stripline technology is the two-dimensional analog of the coaxial cable that is common in high frequency instrumentation. The sensitivity of the stripline configuration will be described in comparison to the more common 3D and planar helix coils, emphasizing in particular on the potential for further miniaturization. Furthermore the thermal characteristics that determine the limits in excitation bandwidth will be discussed. Next the issue of susceptibility broadening will be analyzed as this determines the ultimate resolution that can be achieved. Finally, a preliminary implementation and experimental verification of the stripline configuration will be presented.

2. Stripline modeling

Following Maxwell's equations, the only requirement to achieve a strong RF B_1 field is to create a high RF current density close to the sample volume. A helix is a convenient configuration, but by far not the only one. For example in a saddle coil, the relevant RF fields are generated by straight parallel wire sections. In a stripline the current is fed through a thin metal strip which is placed at some distance above a metal ground plane. A non-radiative closed configuration is realized by placing ground planes both above and below the strip. The magnetic field lines encircle the central strip, so the B_1 field points in opposite directions above and below the stripline. The boundary conditions at the metal surface dictate that the field lines run parallel to this surface and as a result the B_1 field homogeneity is quite good. A secondary consequence is that the current distribution in the strip is nearly homogeneous and the power dissipation is minimized. In Fig. 1 the B_1 field distribution for a micro stripline cross section is shown. In the following this geometry will be analyzed in more detail. It will be shown that for typical sample volumes the sensitivity is comparable or better than that of an optimized helix. The most important advantage, however, is the fact that the stripline design is fully scalable, so that the probe can be adjusted to the specific sample geometry. Since the structures are all single layer lithographically defined, it is straightforward to produce multiple probes on a single semiconductor wafer.

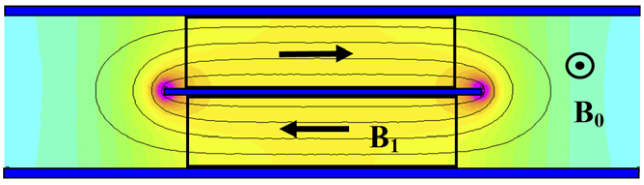

Fig. 1. Schematic cross-section of the stripline design. The RF field B_1 circulates the strip as is indicated by the field lines. The local RF field strength is indicated by the color map (blue corresponds to low B_1 field and red to high B_1 field). Because of the boundary conditions imposed by the metallic planes above and beneath the strip, the magnetic field lines are forced parallel to the surface. The result is a large volume with a homogeneous B_1 field. Suitable sample chambers are indicated by the two black rectangles where the B_1 field is homogeneous within about 10%. Also, the current distribution in the strip is homogeneous thus minimizing electrical losses. For NMR applications one can use the stripline geometry both for excitation and detection by insertion of this structure inside an external field. The static field B_0 can be oriented perpendicular to the cross section shown in the figure (along the stripline axis). The RF current that runs through the central copper strip flows parallel to the static field.

3. Sensitivity

As has been treated by Hoult and Richards [13], the signal to noise ratio in a typical NMR experiment can be written as

$$\mathrm{SNR} = \frac{k_0\left(\frac{B_1}{i}\right)V_S.\omega_0.\frac{1}{\sqrt{2}}.M}{F\sqrt{4k_B T R_{\mathrm{noise}}\Delta f}}$$

where k_0 is a scaling factor accounting for the RF inhomogeneity of the coil, B_1/i is the magnetic field induced in the RF coil per unit current, V_S is the sample volume and ω_0 is the angular RF frequency. The denominator describes the noise determined by the noise factor of the spectrometer (F) and the dissipative losses (R_{noise}) of coil, circuit and sample for the spectral bandwidth Δf. T is the temperature and k_B is Boltzmann's constant. For a nuclear spin system the magnetization (or total magnetic moment per unit volume) is given by Curie's law in the limit for high temperatures:

$$M = N\gamma^2\hbar^2 I(I+1)\frac{B_0}{3k_B T}$$

where N is the number of spins per unit volume, γ the gyromagnetic ratio, I the spin quantum number, B_0 the static field, and h is Planck's constant. The effective sample volume $V'_S = k_0^* V_S$ is defined rather arbitrarily as the volume in which B_1 is within 10% of the maximum value at the center of the coil. With these parameters the signal to noise ratio is given by the simple expression:

$$\mathrm{SNR} = C\frac{B_1 N_S}{i\sqrt{R\Delta f}}$$

where N_S is the number of spins located within the effective volume V'_S. For protons at 600 MHz the constant C equals 1.4×10^{-11} in SI units ($B_0 = 14.09$ T, $T = 300$ K, $\gamma = 0.2675\times10^9$ rad/T s, $I = 1/2$ and $F = 1$, assuming negligible noise contribution from the spectrometer). From this expression it is clear that the way to obtain a good SNR is to create a good filling factor (optimize the number of spins in the homogeneous B_1 volume), maximize the field factor B_1/i and minimize the total electrical resistance.

For reference a helical RF coil is examined. An idealized helical coil is a cylindrical shell with a uniform current density. The RF current will penetrate to a frequency dependent penetration depth δ. For copper at room temperature and at 600 MHz δ equals 2.7 μm. The center field is given by $\frac{B_1}{i} = \frac{\mu_0}{\sqrt{l^2+d^2}}$ and the resistance $R = \rho\frac{\pi d}{l\delta}$, with l the height of the cylinder, d the diameter and ρ the resistivity of copper. The optimum sensitivity is obtained for an aspect ratio $d/l = 1$, and the signal to noise is given by: $\mathrm{SNR} = 0.9\times10^{-16}\frac{N_S}{d\sqrt{\Delta f}}$.

So for a fixed number of spins the signal to noise indeed scales with $1/d$ as predicted by Hoult and Richards [13]. Note that the number of windings n in a helix does not influence the sensitivity. Although the field factor increases linearly in n, the resistance scales with n^2, so both signal and noise are amplified by the same transformation factor. For a typical coil diameter $d = 1$ mm (~1 μl sample volume) 1.1×10^{13} proton spins are needed to obtain an SNR of 1 in a 1 Hz bandwidth. This theoretical detection limit is considerably lower than realized in practice because of additional losses and non-ideal filling factors of a wire coil wound around a capillary sample chamber.

A similar analysis can be performed for the stripline configuration as depicted above. The width of the strip is denoted by w, the length of the stripline by l and the distance between the metallic ground planes by h. For simplicity an aspect ratio $h/w = 1$ is chosen, and $l/w = 2\pi$. For this situation, the sample volume is approximately $2\pi w^3$,which is the same volume as in the case of a helix for $d = 2w$. The strip resistance is identical to that of the cylindrical current shell since $R = \frac{\rho l}{2\delta w} = \frac{\pi\rho}{\delta}$. The B_1 field follows directly from Ampere's law $\oint B\cdot \mathrm{d}s = \mu_0 i$ which yields $B_1/i \approx \mu_0/2w$ and is a factor $\sqrt{2}$ larger than that of the equivalent helix. As a result, the stripline SNR will be a factor $\sqrt{2}$ larger than that of the helix with the same volume. So in contrast to common sense estimates, the optimum RF detection geometry is not the helix. The main physical reason is the fact that for the microstripline the current distribution is homogeneous and runs on both sides of the strip. In a cylindrical shell, the current flows almost exclusively at the inside, so the effective dissipation is doubled and the sensitivity is reduced by $\sqrt{2}$. It is well known among NMR coil builders and electrical engineers that a substantial part of the B_1 field in a helix lies outside the 'region of interest', and that structures such as toroids, striplines and other geometries are more effective in terms of containing the B_1 field. Nevertheless, these alternatives have not yet been realized in commercial probes.

Another way to appreciate the relative sensitivity is to look at some intuitive guidelines. For optimum sensitivity one wants a maximum inductive coupling between sample and RF coil, so all the magnetic energy should be concentrated in the sample volume. For typical helix geometries about half of the magnetic energy is stored within the coil volume. So for a sample located within the helix the remaining half of the magnetic energy is 'wasted'. In contrast, for the stripline in principle the entire volume between the ground planes can be filled with sample thus ensuring maximum inductive coupling.

In addition, the B_1 field homogeneity has to be taken into account. At the end of a helical coil, the field value is reduced to 50% of the value in the coil center, and only about one third of the magnetic energy is stored in the volume where the maximum deviation from the central field is less than 10%. In contrast, for the stripline geometry a much larger percentage of the magnetic energy is stored in the homogeneous field region. For the configuration depicted in Fig. 1 the homogeneous B_1 volume contains more than 50% of the total magnetic energy.

A second guideline is to minimize noise and thus minimize losses in the RF coil. To do so, Eddy currents must

be avoided to ensure a homogeneous current distribution. The stripline is then the most convenient planar analog of the coaxial transmission line and only at the very edges of the stripline an enhanced current density is encountered. This discussion can be made more quantitative by a numerical finite element analysis of the various configurations.

Presently, commercial microcoil probes contain helical RF coils with a diameter of about 1 mm. Some groups have managed to produce smaller size helices with a typical lower limit of 200–300 μm diameter using wire diameters down to 50 μm [2,14–18]. With the present manual technology it seems unlikely that the size can be reduced substantially. At this size, the whole structure and metal wiring become very fragile and mechanical integrity at high RF powers becomes questionable. In Fig. 2 a field map of a 4 turn helix with an inner diameter of 280 μm and a height of 300 μm is displayed. The effective sample volume with a B_1 homogeneity within 10% of the central field, indicated by the thin solid line, represents a volume of 5 nl. The numerical analysis shows that in this volume only 15% of the total magnetic energy is stored. The main parameter that specifies the coil sensitivity $\frac{B_1}{i\sqrt{R}}$ can be calculated directly from the numerical results. The detection limit (LOD) for protons at 600 MHz is defined as the number of spins that are needed to obtain an SNR equal to one for a 1 Hz bandwidth. For this micro helix a LOD of 4×10^{12} proton spins in a 1 Hz bandwidth is calculated. In fact this numerical simulation rather closely follows the ideal shell model with a diameter scaled down by 0.3 from the previously described 1 mm helix. If the susceptibility broadening can be brought down to 0.01 ppm (6 Hz linewidth) then the concentration sensitivity (SNR = 1) for the 5 nl volume equals 3.3×10^{-2} M or 0.16 nanomoles of sample.

A well studied alternative to the helix is the surface microcoil that can be produced by lithographic techniques. In Fig. 2b the field profile of a surface coil with three windings is shown. Again, the cylindrical 5 nl sample volume in which the field is homogeneous within 10% from the center field is indicated by the thin solid line. For this configuration only 4% of the total magnetic energy is concentrated in the sample volume. The LOD is found to be 7×10^{12} proton spins per $\sqrt{\text{Hz}}$, which is nearly a factor of 2 less than the helix above. This is mainly due to the fact that the outer windings contribute less to the central field and contribute substantially to a higher coil resistance. In practical designs it is not straightforward to obtain a low loss connection to the inner winding, but this is not even included in the numerical calculation. Note that adding extra windings does enhance the central field, but the sensitivity remains nominally the same. Because of Eddy currents the coil sensitivity actually reduces with an increased number of windings.

Finally, in Fig. 2c the magnetic field distribution for a planar stripline with a width of 100 μm is depicted. In this case, the homogeneous volume, represented by the two boxes above and below the strip, contains more than 50% of the total magnetic energy and the LOD is found to be 3×10^{12} proton spins per $\sqrt{\text{Hz}}$ for a strip length of 1 mm. This is again consistent with the estimates based on the idealized model and confirms that the stripline configuration can indeed be more sensitive than the helix. At the proton concentration of water, this corresponds to a detectable volume of 45 fl for a 1 Hz bandwidth (SNR = 1 for a single scan) equivalent to a spherical volume of 4 μm in diameter. A note of caution is in order however, in this analysis it is assumed that the spectrometer components (preamplifiers, etc.) do not add to the overall noise performance. The very low impedance of the stripline may however put some constraints on the matching conditions to the 50 Ω outside world and additional noise contributions may become important.

4. RF power handling and excitation bandwidth

Helical microcoils offer high sensitivity because of their field factor (high B_1 field per unit current amplitude). This implies that the excitation bandwidth is also large, making

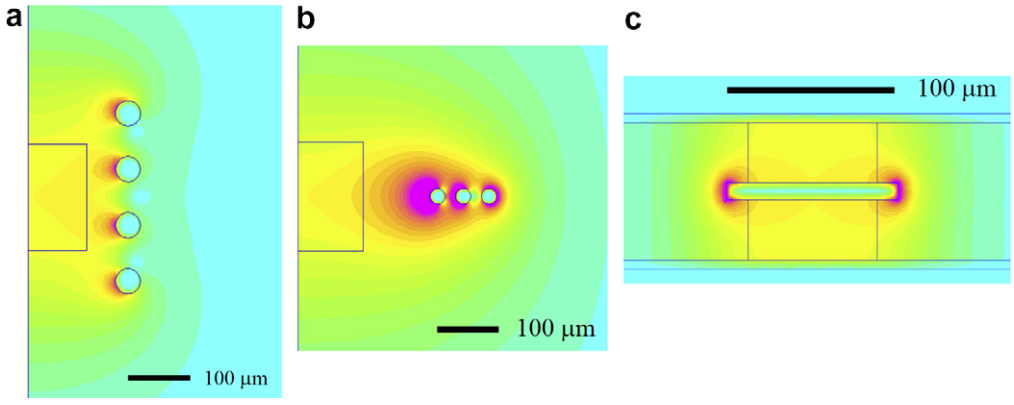

Fig. 2. (a) Axial RF field map (blue corresponds to low B_1 field and red to high B_1 field) for a micro helix coil at an RF frequency of 600 MHz. The cylindrical symmetry axis is at the left of the figure. The radius of the coil is 140 μm, the length is 300 μm and the wire diameter 40 μm. (b) Axial RF field map for a planar micro helix coil at an RF frequency of 600 MHz. (c) Axial RF field map for a microstripline at an RF frequency of 600 MHz. The width of the strip is 100 μm, thickness 20 μm and arbitrary length.

it possible to use short $\pi/2$ pulses for wide-line solid-state NMR applications [18]. On the other hand, for narrow-band applications one can work with extremely low RF powers, typically in 0.01–1 W range, opening the way for low cost integrated spectrometers. The stripline configuration as described above acts basically as a one turn coil, so the field factor is generally lower. Nevertheless, the improved heat transfer for this configuration allows a very high excitation bandwidth. This is not only a great benefit for inductively detected NMR but can also reduce heat-induced problems encountered in magnetic resonance force microscopy where the rf coil is driven in quasi CW mode for periodically inverting the spins adiabatically. The heat produced in the RF coils is a major noise source deteriorating signal-to-noise.

Some estimates toward the limits in RF power handling can be made. As a first approximation it is assumed that losses are dominated by the electrical resistance of the microstripline. For a freestanding wire the heat that is generated will be transported by thermal conduction through the wire towards the bulky contact pads. For simplicity it is assumed that these heat-sinks remain at ambient temperature. For a properly matched circuit all the external RF power will be dissipated in the microstripline. The Fourier heat equation for a strip with constant cross section leads to a quadratic solution of the temperature as a function of the distance from the center of the strip. For the 100 μm × 1 mm (5 nl) stripline described above, this translates to a 200 kHz proton excitation bandwidth at a dissipated power of only 20 mW and a CW heating profile with a maximum temperature raise of 9 K above ambient at the center of the strip. A graphical representation of the temperature profile is plotted in Fig. 3. This heating can be further reduced by shortening the strip, increasing the thickness (more efficient heat transport to the contacts) or by using a substrate material with a good thermal conductivity. For a strip in good thermal contact to a pure Si substrate, the three-dimensional heat diffusion into the substrate leads to a strong reduction of the maximum temperature, and a 200 kHz CW excitation can be realized with only 0.5 °C temperature increase at the center of the strip. This opens the possibility for very high RF field experiments; on pure Si substrates the strip safely allows sustained 1 MHz or higher B_1 fields in cross-polarization or decoupling sequences. For very small samples one can reduce the microstripline length and a CW 10 MHz B_1 field can be generated with acceptable heating tolerances. Temperature heating effects under short pulsed conditions are not critical and pulsed excitation bandwidths above 10 MHz should be feasible. Note that these microstripline probes have a low loss and thus a rather high Q factor. The effective excitation bandwidth is therefore limited by the overall probe Q factor.

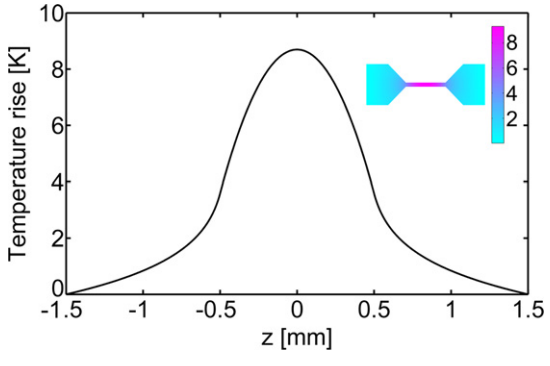

Fig. 3. Temperature distribution in a freestanding 100 μm wide stripline subjected to an RF power resulting in 200 kHz proton B_1 field strength. The maximum temperature rise at the center of the strip under CW conditions is 9 K. A freestanding helix that produces the same B_1 field would heat up to about twice this temperature. Inset: temperature distribution of the strip in good thermal contact to a pure silicon substrate. The maximum temperature rise at the center is 0.5 K in this case.

For comparison, the 5 nl helical coil described earlier would produce a higher B_1 field per unit current, but as in the case of the sensitivity, the B_1 field per unit power is in fact lower than in the case of the 5 nl microstripline. In this example for the same B_1 field and comparable metal cross sections, the temperature rise in a helix is a factor 20 higher than that of the equivalent stripline. A critical point here is also that the thin wire has to be soldered onto the massive contact pads. This inevitably gives rise to additional contact resistances and less ideal cooling conditions. The microstripline can be produced lithographically, however, without the need to solder these small components and thermal breakdown of the RF structure is much less of a problem.

Finally, a point of concern in NMR of biological samples with high salt concentrations is the dielectric sample heating due to RF currents induced in the sample. In the case of the stripline structure as depicted above, the dominant electrical field component is perpendicular to the strip surface. By designing the structure as a $\lambda/2$ mode structure, this electrical field is zero at the center of the strip due to the symmetry of the design. Preliminary numerical simulations have shown that for liquid aqueous samples the maximum electrical fields near the ends of the central stripline are about a factor 10 lower than in a comparable helix that generates the same B_1 field.

5. Susceptibility effects and resolution

Despite the obvious advantages of microcoils in terms of sensitivity and excitation bandwidths, their penetration into mainstream NMR has been rather slow. This is mostly due to the compromises that must be made in spectral resolution. High sensitivity dictates a high filling factor, so the RF coil must be in close contact with the sample space. Inevitably, the magnetic susceptibility of the metal wire is different from that of the sample holder and distortions in the B_0 field lead to a reduced resolution. The small dimensions of the microcoil lead to field gradients that vary over very short distances and the resulting field profile can-

not easily be shimmed by macroscopic shim coils far away from the sample.

Commercial microcoil probes rely on immersion of the coil structure in a special fluid which has the same susceptibility as copper [4]. The successful susceptibility matching of these solenoidal coils has lead to extensive applications for example in the field of high-throughput screening. In contrast to the helix, the microstripline has some properties that make the susceptibility problem much easier to handle. The first aspect is that the axis of the stripline can be oriented parallel to the static field B_0. The magnetization of the copper strip is homogeneous and oriented parallel to the external field. From Maxwell's equations it is easy to see that for an infinitely long strip, there is no field inhomogeneity at the position of the sample and thus the ultimate resolution provided by the magnet should be attainable. In addition, since the sample is small and has a nearly one-dimensional shape along the axis of the field, it is easy to find optimum shim parameters. In the inset of Fig. 4 the local field variations for a plane just above a microstripline are plotted, including the contact pads that are tapered at an angle of 45°. In the center part, the susceptibility broadening is limited to below 0.1 ppm. Fig. 4 shows the static field for a trace along the z-axis at a small distance above a microstripline. As usual there is a tradeoff between optimum sensitivity and optimum resolution. If a higher resolution is required one can introduce susceptibility matched plugs to limit the detection volume to the center part of the microstrip, where the B_0 field is more homogeneous. In the case of a very short strip advantage can be taken of a special property of the dipole field. If the contact pads are cut symmetrically along the magic angle (54.7°) with the sample axis parallel to the static field, then the edges produce a minimum gradient at the sample position. In this case, the quadratic term in a Taylor expansion of the field distortion at the sample center becomes zero.

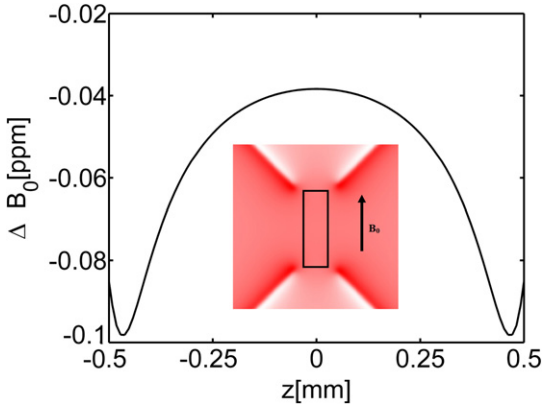

Fig. 4. B_0 field distribution along the z-axis at a distance of 50 μm above the axis of a microstripline with a width of 100 μm, length 1 mm and a metal thickness of 10 μm. The field inhomogeneity is below 0.05 ppm for the central part of the strip. Inset: B_0 field profile at a plane just above a microstripline. At the edges of the contact pads we find a considerable field gradient with a maximum deviation from the center field of approximately 2 ppm. At the sample position, indicated by the solid rectangle, the field deviations are well below 0.1 ppm.

Susceptibility matching can also be used in the case of the stripline, for example by using a multilayer conductor with a positive susceptibility material sandwiched between two copper layers. In this case the whole structure, including contact pads can be made of effectively zero susceptibility material. This is similar to the well known technique to use zero susceptibility wire for high resolution probes [4]. The advantage for planar structures is that production is much easier, more reproducible and better adapted to numerical simulation techniques. A second option is to replace the copper that is etched away in the lithographic process by some other non-conducting material that has the same magnetic susceptibility as copper. For example PPS, *p*-phenylene sulfide, has a volume magnetic susceptibility of -9.17×10^{-6} (in SI units) compared to -9.65×10^{-6} for copper. As an alternative, teflon has an approximate volume susceptibility of -10.5×10^{-6}. In the cases of a closed sandwich configuration one could also fill the voids by susceptibility matching fluids as is common in capillary helical microcoil probes. Simulations show that with common materials such as Teflon to fill the etched channels a theoretical line broadening induced by the probe is predicted to be below 1 Hz.

6. Practical implementation and preliminary results

A typical property of microcoils in general and microstriplines in particular is that both the inductance and the resistance are very low. Therefore special attention to minimize losses at the contacts and to obtain good matching to the external 50 Ω circuit is required. A convenient resonator is that of a $\lambda/4$ structure with the stripline inserted as a short at one side of the resonator and a capacitive coupling and tuning network near the open side of the resonator. In Fig. 5a the electrical circuit for a double resonance probe with a 600 MHz proton channel and variable frequency X-channel is shown. The coupling to the $\lambda/4$ resonators is chosen at a convenient point to achieve the best matching conditions. Tuning is realized by the insertion of variable length dielectric stubs inside the coaxial resonator structures. Typical Q factors for this design are between 80 and 100. Fig. 5b shows the probe with the stripline located at the very top. For this prototype, a 1 mm stripline with a width of 500 μm was produced photolithographically using low-loss Teflon-based printed circuit board (PCB) material (Rogers RT/duroid 5870). Contact masks were used with high resolution structure definition. The wet etching allows structures down to about 20 μm in size. The PCB thickness was 0.254 mm, with a copper cladding of 35 μm. The sample chamber was machined in a second layer of PCB, where the top copper layer was removed (not shown). The bottom copper layer of the sample holder acts as the second ground plane and closes the symmetric stripline configuration.

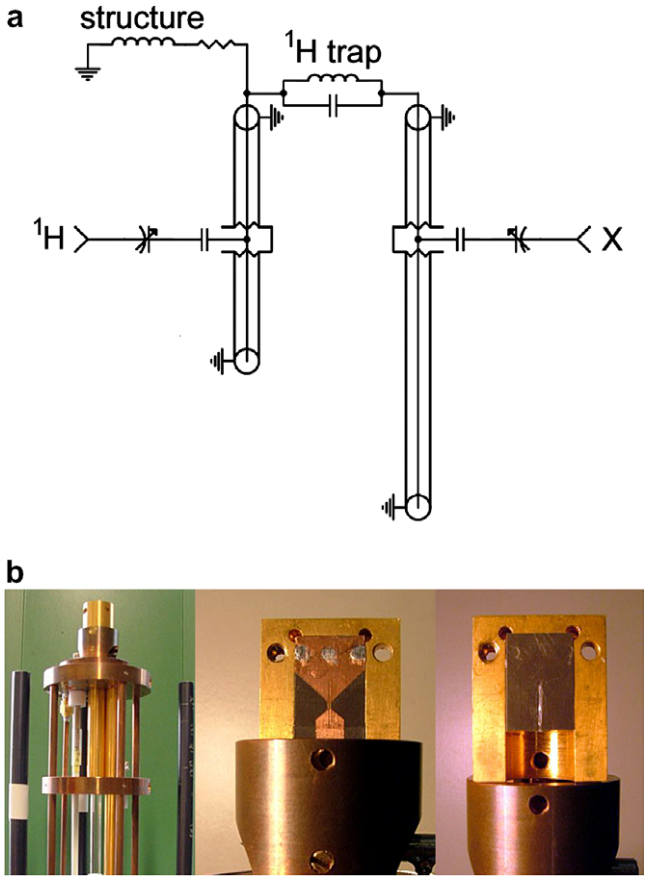

Fig. 5. (a) Electrical circuit for a double resonant probe with a 600 MHz proton channel and variable frequency X-channel. The stripline is represented by the inductor structure at the left upper side of the schematic. The coupling to the $\lambda/4$ resonators is chosen at a convenient point to achieve the best matching conditions. Tuning is realized by the insertion of variable length dielectric stubs inside the coaxial resonator structures. Typical Q factors for this design are between 80 and 100. (b) Actual photograph of the prototype double tuned stripline probe, showing the stripline structure (center) and the sample holder with capillary (right) and ground planes on both sides (not shown).

Solid and liquid-state samples were used to determine the performance of this prototype probe. The first sample was a small 1 mm diameter disk of silicone rubber placed on top of the stripline. The total sample volume was 200 nl in this case. To determine the field strength and rf-homogeneity proton nutation spectra were obtained for the narrow methyl-proton signal of the silicone rubber. The nutation curve for the silicone sample gives an rf field strength of 90 kHz at an RF power of 5 W. The 810° over 90° pulse ratio is 62% (Fig. 6), which is acceptable considering the fact that the sample diameter is slightly larger than the width of the strip.

A very interesting application area for solid-state NMR is the study of thin film material. To explore this capability a film of commercial polyethylene based packaging material was placed over the stripline. This 10 μm thick foil corresponds to an effective sample volume of approximately 10 nl. A proton single-pulse excitation experiment gave an SNR of 165 in as little as 4 scans. Fig. 7 shows a deconvolution of the spectrum which has a typical three component proton wide-line spectrum. In accordance with proton wide-line studies of LDPE [19] the spectrum can be deconvoluted into a broad Gaussian peak, a Lorentzian with intermediate line width and a narrow Lorentzian. These are attributed, respectively, to the rigid, semi-rigid and soft amorphous phases of the polymer. These results demonstrate the sensitivity of the stripline for thin-film wide-line NMR spectroscopy. This configuration might also be exploited for highly resolved materials imaging.

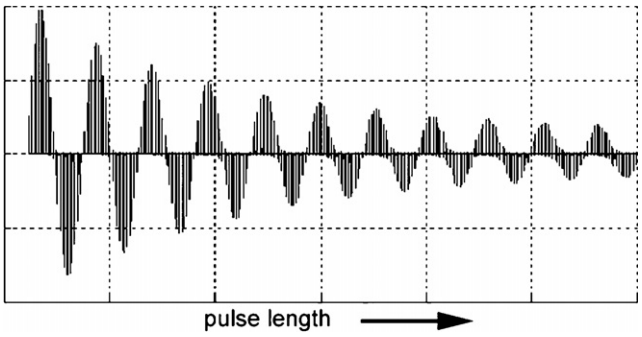

Fig. 6. Proton nutation signal at 600 MHz for a 200 nl silicone rubber sample in an approximately cylindrical geometry of 500 μm diameter and 250 μm thickness on a 500 μm wide stripline. The 810/90 ratio is 62%.

To demonstrate liquids capabilities a thin 110 μm inner diameter capillary filled with pure ethanol was placed on the stripline, with the capillary extending over the wide contact areas. The nutation spectrum in this case shows that the RF field is considerably reduced above these contact pads, moreover the sample above the pads seriously affects the resolution. The sample volume located above the central part of the stripline is about 12 nl in this case. The proton rf field strength was 140 kHz at a source power of 5 W. With the experimentally determined Q factor of the probe and the simple model based on Ampere's law an rf field strength of 150 kHz is expected, in good agreement with the experimental observations. Also the B_1 homogeneity is in agreement with the theoretical predictions.

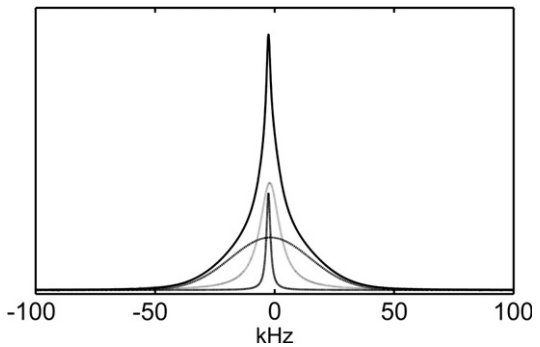

Fig. 7. Proton wide-line spectrum of a PE foil (thickness 10 μm, volume 10 nl) measured at 14.1 T (600 MHz; 128 scans). The experimental (dotted) spectrum overlaps perfectly with a deconvolution of the spectrum in a linear combination of a broad Gaussian and intermediate and narrow Lorentzian lines. The separate components are assigned to fractions with distinct differences in molecular mobility.

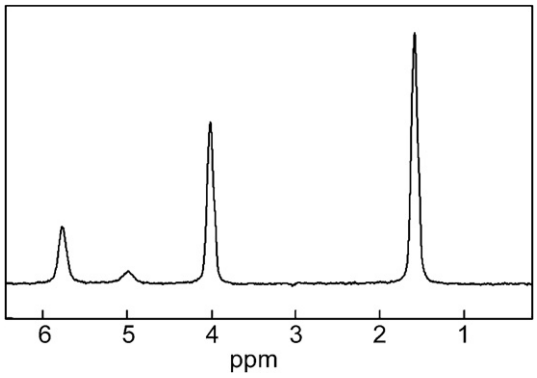

Fig. 8. Single scan proton spectrum of a 12 nl ethanol sample obtained at 600 MHz (14.1 T) in the prototype stripline probe. The spectrum was obtained by subtracting a 180° spectrum divided by two from a single scan spectrum excited under normal 90° pulse conditions, in this way signals from material above contact pads that experience a rather low RF field strength are eliminated from the overall signal.

A spectrum obtained for the 12 nl ethanol sample is shown in Fig. 8. To eliminate the broadened and shifted signal from ethanol above the contact pads, the spectrum was obtained by subtracting half of a 180° spectrum from a single scan spectrum excited under normal 90° pulse conditions. In this way signals that experience rather low rf field strength are eliminated from the overall signal. Clearly this can be done more efficiently by implementing composite pulse that select for homogeneous B_1 field [20]. The single scan SNR equals 440 as determined in the time domain. This translates to an experimental detection sensitivity (LOD) of 1.5×10^{13} spins per $\sqrt{\text{Hz}}$. The theoretical prediction for this geometry (including the spreading resistance of the contact areas) amounts to 1.2×10^{13} spins per $\sqrt{\text{Hz}}$, which is in reasonable agreement with experiment. Note that the present capillary covers only 20% of the stripline width, so an improvement by a factor two in sensitivity is rather straightforward. The final and possibly most important parameter is the spectral resolution that can be obtained. For the proton difference spectrum of ethanol shown in Fig. 8 a line width of 50 Hz, corresponding to a resolution of 0.08 ppm, is obtained. Although this is not true high resolution, this is sufficient to already study e.g. reaction kinetics for many reactions that are performed in microfluidic devices. It should furthermore be noted that the present prototype probe was not designed for very high resolution work, and no effort was made to introduce susceptibility matching. The present results represent a basic starting point for the spectral resolution that can be obtained in stripline probes.

7. Discussion and conclusions

The present prototype is a double resonance system (H and X), where the basic stripline part is cheap and easily replaceable (plug and play). With this prototype the main conclusion from the design calculations are confirmed: very high sensitivity, high RF field strength with good thermal characteristics and good B_1-homogeneity characteristics over a large volume of the available sample space around the structure. Further optimizations are underway to obtain the ultimate spectral resolution which should be accessible due to an intrinsically low susceptibility distortion of the static field.

One can easily optimize the stripline configuration for various sample sizes and concentrations. For example in the case of microfluidic on chip analysis the aim is to optimize signal to noise ratios for low concentration solutions. The main guideline is to have a sufficient number of nuclear spins in the detection volume. This number is limited by the acceptable sample volume and concentration. Assuming that 5 μl is an acceptable sample volume, the discussed 5 nl design can be scaled up by a factor 10 in size (1 mm strip width, 10 mm length). The absolute sensitivity decreases linearly with this scale factor, but the concentration sensitivity goes up quadratically with the scale factor and one may expect that a 10^{-1} M solution can be detected with a signal to noise ratio of about 25 in a single scan (assuming again a spectral linewidth of 0.01 ppm). This would e.g. allow relatively fast 'realtime' screening of HPLC output flows or the study reaction kinetics 'on chip'. In principle, the stripline configuration is better adopted to measure solutes in microfluidic channels compared to surface helix coils which are better matched to a cylindrical sample chamber.

Many interesting samples are two-dimensional in nature, such as coatings, epitaxial layers, MBE grown films, etc. With helical NMR detection coils these samples are difficult to handle. Removing the surface layer and transfer of the resulting powder to a cylindrical sample holder could result in structural changes and information about preferential orientation and ordering may be lost. Sometimes it is possible to cut the substrate in bars and stack these in the cylindrical NMR probes. Apart from the low filling factor, this will lead to destruction of the sample. Moreover, lossy and/or metallic substrates are difficult to handle with this procedure. Striplines give additional options, however; it is imaginable to replace one of the metal ground planes with such a coated metallic substrate and detect the nuclear spins in the surface layer non-destructively maintaining the full information content. In fact one can even think of a xy scanning stage where the local information is measured as a function of the position.

A third sample geometry is encountered for single crystals or biological fibers that are inherently small in size, difficult or expensive to synthesize because of isotopic labeling, etc. For a dendrite crystal the width and length of the stripline can easily be adjusted to match the sample dimensions. This will improve the signal to noise performance by factors $\sim 1/\sqrt{w}$ and $1/\sqrt{l}$, where again w is the width of the strip and l is the corresponding length. A typical lower limit is the situation when the cross section of the strip becomes comparable to the RF penetration depth and the gain in field factor is thwarted by the fast increase of the resistance. For a needle like crystal of $(10\ \mu\text{m})^2$ cross sec-

tion and 1 mm length a LOD of about 1×10^{12} spins per $\sqrt{\text{Hz}}$ is expected for abundant spins such as protons. Looking at quasi-cubic crystals of approximately $(10\ \mu\text{m})^3$ both width and length of the strip can be reduced to obtain a theoretical LOD of 3×10^{11} spins per $\sqrt{\text{Hz}}$.

In summary, the proposed stripline configuration represents a simple and effective design for mass-limited NMR samples that is easy to produce with lithographic methods. Attractive points are the fact that the sensitivity can be competitive with optimized helical coils and many of the problems encountered in planar helices are absent. In essence, the high sensitivity and high B_1 field of the helical microcoils is conserved. The simple planar design allows a quantitative modeling of both static and high frequency components using analytical or 2D finite element analysis. A strong advantage of the present design is its scalability. The same approach can be used both for large surface layers, small diameter cylindrical samples or tiny micro crystals.

Further developments of the stripline design are underway. Currently preliminary experiments with a microfluidic chip with integrated microstrip are carried out. By integrating the entire resonator and matching circuits on a single chip we hope to minimize the external losses and integrate microfluidics with NMR circuitry in a pure lithographic planar process. Without critical discrete elements this ultimately may lead to NMR probes that are cheap disposable consumables.

8. Experimental

All NMR experiments were carried out on a Chemagnetics CMX-Infinity 600 solid-state NMR spectrometer, operating at a magnetic field strength of 14.1 T. Silicone rubber was of a generic household type and used without further treatment. Ethanol (pro analysis 96%) was obtained from Merck. The prototype stripline probes were made lithographically from Teflon-based high frequency laminate (RT duroid 5870, Rogers). All data processing and spectral deconvolution was done using the matNMR processing package [21].

High frequency finite element analyses were carried out using FEMM (David Meeker, dmeeker@ieee.org), HFSS (Ansoft) and CST Microwave Studio (CST GMBH) for both 2D and 3D simulation of the RF mode structure and evaluation of resistive and dielectric losses, optimal coupling conditions and tuning. The static field distortion and susceptibility effects were calculated for the full structures using a dedicated C-program using CVI (National Instruments). The thermal analysis was performed using both analytical calculations in Maple (Maplesoft) and 2D numerical modeling in Matlab (Mathworks).

Acknowledgments

We acknowledge the support and feedback in many illuminating discussions with J.W.M. van Os and G.E. Janssen. We thank Dr. J. Jansen and Dr. R. Dekker for their early support and interest for this project. This project is partially funded by the Dutch NWO ACTS–POAC program and the FOM-Philips 'Laboratorium zonder Muren' program.

References

[1] N.A. Wu, T.L. Peck, A.G. Webb, R.L. Magin, J.V. Sweedler, H-1-NMR spectroscopy on the nanoliter scale for static and online measurements, Analytical Chemistry 66 (1994) 3849–3857.
[2] D.L. Olson, T.L. Peck, A.G. Webb, R.L. Magin, J.V. Sweedler, High-resolution microcoil H-1-Nmr for mass-limited, nanoliter-volume samples, Science 270 (1995) 1967–1970.
[3] D.L. Olson, Microflow NMR: concepts and capabilities, Analytical Chemistry 76 (2004) 2966–2974.
[4] A.G. Webb, Radiofrequency microcoils in magnetic resonance, Progress in Nuclear Magnetic Resonance Spectroscopy 31 (1997) 1–42.
[5] A.G. Webb, Microcoil nuclear magnetic resonance spectroscopy, Journal of Pharmaceutical and Biomedical Analysis 38 (2005) 892–903.
[6] J. Dechow, A. Forchel, T. Lanz, A. Haase, Fabrication of NMR—microsensors for nanoliter sample volumes, Microelectronic Engineering 53 (2000) 517–519.
[7] J.D. Trumbull, I.K. Glasgow, D.J. Beebe, R.L. Magin, Integrating microfabricated fluidic systems and NMR spectroscopy, IEEE Transactions on Biomedical Engineering 47 (2000) 3–7.
[8] C. Massin, C. Boero, F. Vincent, J. Abenhaim, P.A. Besse, R.S. Popovic, High-Q factor RF planar microcoils for micro-scale NMR spectroscopy, Sensors and Actuators a-Physical 97-8 (2002) 280–288.
[9] H. Wensink, F. Benito-Lopez, D.C. Hermes, W. Verboom, H. Gardeniers, D.N. Reinhoudt, A. van den Berg, Measuring reaction kinetics in a lab-on-a-chip by microcoil NMR, Lab on a Chip 5 (2005) 280–284.
[10] K. Ehrmann, M. Gersbach, P. Pascoal, F. Vincent, C. Massin, D. Stamou, P.A. Besse, H. Vogel, R.S. Popovic, Sample patterning on NMR surface microcoils, Journal of Magnetic Resonance 178 (2006) 96–105.
[11] P.J.M. van Bentum, J.W.G. Janssen, P.M. Kentgens, Towards nuclear magnetic resonance μ-spectroscopy and μ-imaging, Analyst 129 (2004) 793–803.
[12] Y. Maguire, I.L. Chuang, S. Zhang, N. Gershenfeld, Ultra-small-sample molecular structure detection using microslot waveguide nuclear spin resonance, PNAS 104 (2007) 9198–9203.
[13] D.I. Hoult, R.E. Richards, The signal-to-noise ratio of the nuclear magnetic resonance experiment, Journal of Magnetic Resonance 24 (1976) 71–85.
[14] D.L. Olson, M.E. Lacey, J.V. Sweedler, High-resolution microcoil NMR for analysis of mass-limited, nanoliter samples, Analytical Chemistry 70 (1998) 645–650.
[15] A.C. Wright, T.A. Neideen, R.L. Magin, J.A. Norcross, Evaluation of radio frequency microcoils as nuclear magnetic resonance detectors in low-homogeneity high-field superconducting magnets, Review of Scientific Instruments 69 (1998) 3938–3941.
[16] D.A. Seeber, R.L. Cooper, L. Ciobanu, C.H. Pennington, Design and testing of high sensitivity microreceiver coil apparatus for nuclear magnetic resonance and imaging, Review of Scientific Instruments 72 (2001) 2171–2179.
[17] M. Kakuta, D.A. Jayawickrama, A.M. Wolters, A. Manz, J.V. Sweedler, Micromixer-based time-resolved NMR: applications to ubiquitin protein conformation, Analytical Chemistry 75 (2003) 956–960.
[18] K. Yamauchi, J.W.G. Janssen, A.P.M. Kentgens, Implementing solenoid microcoils for wide-line solid-state NMR, Journal of Magnetic Resonance 167 (2004) 87–96.

[19] C. Hedesiu, D.E. Demco, R. Kleppinger, A.A. Buda, B. Blumich, K. Remerie, V.M. Litvinov, The effect of temperature and annealing on the phase composition, molecular mobility and the thickness of domains in high-density polyethylene, Polymer 48 (2007) 763–777.

[20] A. Bax, A spatially selective composite 90° radiofrequency pulse, Journal of Magnetic Resonance (1969) 65 (1985) 142–145.

[21] J.D. van Beek, matNMR: a flexible toolbox for processing, analyzing and visualizing magnetic resonance data in Matlab(R), Journal of Magnetic Resonance 187 (2007) 19–26.